Deciphering unsaturated soil behaviour and transitions across all capillary regimes

Richard Wan*[,1], Nabil Younes[2], Antoine Wautier[3], Olivier Millet[4], and Francois Nicot[5]

[1]*Department of Civil Engineering, University of Calgary, Calgary, Canada*
[2]*LMGC, Univ Montpellier, CNRS, Montpellier, France*
[3]*Unité de Recherche RECOVER-INREA, Aix-Marseille Université, Aix-en-Provence, France*
[4]*Laboratoire des Sciences de l'Ingénieur pour L'Environnement - LaSie, La Rochelle Université, La Rochelle, France*
[5] *ISTerre, Université Savoie Mont Blanc, Chambéry, France*
**Corresponding author's email:* wan@ucalgary.ca

Abstract: The paper examines the behaviour of unsaturated soil as air and water progressively penetrate or exit pores during all water saturation regimes and transitions. Since the physics underlies the collective interactions of water, air and solid particles in the pore space, a numerical framework is adopted where many-body interactions are considered using discrete element modelling for solid grains coupled with air and water dynamics described by the Lattice Boltzmann method. Such a computational approach provides a viable route to model the complex formation, coalescence or rupture of liquid bridges in the pore network. Computing the dynamics of water or air invasion ultimately unravels the role of capillary-induced stresses during wetting, including retention characteristics of an unsaturated soil. With this picture of a system dominated by elementary pore and grain physics, we anticipate that these aspects can be homogenized to the continuum scale for a detailed stress-deformation analysis of geostructures subjected to wetting and drying cycles.

Introduction

Today, the behaviour of saturated soils is undeniably very well understood ever since the early days of Karl Terzaghi who brought soil mechanics—especially the principle of effective stress—to geotechnical engineering. However, extending our understanding to the behaviour of unsaturated soils becomes more complicated since water, air and other gases coexist in the void space. These additional fluids bring intricate interactions between the various constituents and the soil grains, which raises thorny issues such as the characterization of the various partial stresses, interfacial tension, and the stresses controlling strength in the diverse regimes of water saturation [1, 2]. In this day and age of climate change where unsaturated soils in geotechnical engineering are being more appreciated, principles of mechanics and hydraulics must be properly extended to include fundamental interfacial physics and thermodynamics. In this regard, the stress-strain-hydrologic behaviour of natural or engineered soils is strongly dependent on

interfacial interactions in the form of a contractile skin in between the phases that creates surface tension effects.

Although the literature on unsaturated soils is richly well-developed nowadays [3, 4, 5], several basic questions of continuing importance still have to be answered such as describing the crossing of all water saturation regimes as a soil is cyclically wetted and dried. This is in obvious connection with the role of climate on geostructures such as slopes, embankments and dams which consist of compacted engineered soils, hence unsaturated. Water in various proportions in the soil's interstices vastly modifies its mechanical properties—its state may transition from that of a bulk solid to a fluid that flows spontaneously, producing a wetting collapse. When dried, soils lose moisture and shrink, eventually causing cracking

To motivate the discussion further, let's recall the four water saturation (capillary) regimes that exist in a soil starting from the dry state: (1) pendular, where particles are cohesively held by isolated liquid bridges; (2) funicular, where the liquid bridges coalesce, engulfing a few particles; (3) capillary, where liquid with some air occlusions invades the entire void space under capillary action; and (4) the fully saturated condition with exclusively liquid in the void space such that particles could be fully immersed as in a mud slurry.

It turns out that many geostructures undergo swings in the above-mentioned capillary regimes during exposure to climatic fluctuations that will invariably change their mechanical characteristics to eventually induce disastrous structural failure, putting capillary regime changes in the spotlight. Transitions between the various capillary regimes are directly linked to structural failures observed in the field which can only be analyzed at the microscale (grain/pore). This means that we must formally—instead of phenomenologically—describe the different capillary regimes and transitions in a unified mathematical framework to precisely model failure in unsaturated geostructures.

In the literature, the transition from dry to pendular regime has been amply studied [1, 6], whereas in this work the more challenging transition from pendular to funicular regime is investigated. Such a transition certainly causes a sudden drop in effective stress followed by irreversible deformations and a suction change-induced plasticity. It also triggers material instabilities such as internal erosion and liquefaction. While many studies have focused on the failure aspects, existence of an effective stress [7, 8], retention properties, and drying or wetting, a proper modelling of capillary forces during wetting/drying cycles through distinct transitions in capillary regimes remains elusive today. Moreover, failure in unsaturated soils manifests itself through many more subtle modes besides wetting collapse, mandating a robust framework such as the second-order work for analysis [9].

In addressing the central issue of modelling the full physics and transitions entirely across all capillary regimes, the present paper starts off with a brief introduction of the Lattice-Boltzmann Method (LBM) [10] to examine the multiphase flow at the pore scale in complex geometries, while the motion of the solid particles is being described by the Discrete Element Method (DEM) [11] based on solving Newton's second law of motion. Then, the detailed formation, merging and rupture of liquid bridges between particles are numerically modelled, revealing the underlying micro-physics of water retention, capillary forces and hysteresis in wetting and drying cycles.

Multiphase Lattice-Boltzmann

The study of multiphase flow within soil's void space at the microscale requires us to abandon the treatment of fluids as continua, but rather represent their discrete molecular nature as well as their collective behaviours, especially interactions with the solid grains. Modelling the details of the micro scale where molecules move under various forces would be very complicated as could be done using a molecular dynamics approach. Instead, to reduce the high dimensionality of the problem, the Lattice Boltzmann Method (LBM) is used.

There is an abundant literature on the Lattice Boltzmann method [10] which has emerged as a powerful tool in computational fluid dynamics and material science. There are, however, limitations and challenges in the application of the method, particularly in compressible fluids and multiphase physics, e.g. [12]. Herein, our contribution is to include capillary forces and an algorithm for phase change to address evorporation and condensation in liquid bridge dynamics inside a granular soil [13].

To put things into perspective, we give a succinct description of the method as background material to support the numerical simulations that will be described later. The Lattice Boltzmann Method essentially looks at an intermediate scale where ensembles of fluid molecules occupy a small volume element compared with the size of the problem, but large enough to capture very many molecules. The objective is to have a sufficient description of the average properties of the molecules in this element. A statistical description introduces a probability distribution function $f(\boldsymbol{\xi}, \boldsymbol{r}, t)$ that is defined as a function of microscopic velocity $\boldsymbol{\xi}$, position vector $\boldsymbol{r}$ and time t by considering an element in the velocity space $d\xi^3 = d\xi_x.d\xi_y.d\xi_z$ with sides $d\boldsymbol{\xi}$ located at velocity $\boldsymbol{\xi}$. Thus, the PDF is the density of molecules in the six-dimensional "phase-space" combining velocity and space. To describe the dynamics of two fluids, i.e. water and air, including interfaces, an additional PDF $g(\boldsymbol{\xi}, \boldsymbol{r}, t)$ is introduced. In particular, by writing the first moment of g gives the phase field ϕ to determine the partitioning of the phase densities, i.e.

$$\phi(\boldsymbol{r}, t) = \int g(\boldsymbol{\xi}, \boldsymbol{r}, t)\, d\xi^3 \text{ where } \phi = \frac{\rho - \rho_g}{\rho_l - \rho_g} \tag{1}$$

Basically, the phase field $\phi = 0$ refers to gas and 1 to liquid and anything in between is the interface. At thermodynamic equilibrium, the phase field distribution is mathematically described by a smooth Heaviside function (sigmoid function) which controls the width of the interface, hence its sharpness. Calculating the phase field ϕ over the domain of interest, the density can be determined from respective liquid and gas densities to uncover the spatial distribution of the phases and the topology of the interfaces.

Furthermore, the second moment of the probability distribution function f coincides with the momentum, and hence the macroscopic velocity $\boldsymbol{u}$ can be retrieved:

$$\rho(\boldsymbol{r}, t)\, \boldsymbol{u} = \int \xi\, f(\boldsymbol{\xi}, \boldsymbol{r}, t)\, d\xi^3 \text{ where } \boldsymbol{u} = \{u_x, u_y, u_z\} \tag{2}$$

Writing the conservation of mesoscopic particles in both space and the phase-space gives way to two Boltzmann equations which consist of a streaming part where particles move over a

lattice and a second part (Ω) describing interactions with other particles through collision, i.e.

$$\frac{\partial f}{\partial t} + \boldsymbol{\xi}.\boldsymbol{\nabla} f = \Omega(f); \qquad \frac{\partial g}{\partial t} + \boldsymbol{\xi}.\boldsymbol{\nabla} g = \Omega(g) \tag{3}$$

Proper choices of collision operators Ω make the equations converge to the Navier-Stokes and Allen-Cahn equations respectively, i.e.

$$\begin{aligned} \rho\left[\frac{\partial \boldsymbol{u}}{\partial t} + \boldsymbol{\nabla}.(\boldsymbol{u}\otimes\boldsymbol{u})\right] &= -\boldsymbol{\nabla} p + \boldsymbol{\nabla}.\boldsymbol{\tau} + \boldsymbol{F}_s \\ \frac{\partial \phi}{\partial t} &= \boldsymbol{\nabla}.\left[M\left(\boldsymbol{\nabla}\phi - \lambda\frac{\boldsymbol{\nabla}\phi}{|\boldsymbol{\nabla}\phi|}\right)\right] \end{aligned} \tag{4}$$

In the Navier-Stokes equation, we have added a surface tension term to represent capillary effects. Essentially, a potential form is postulated based on previous works in the literature where the surface tension term F_s is related to the gradient of the phase field function ϕ through a chemical potential μ_ϕ defined as the minimum of the mixing energy. The second equation is the Allen-Cahn equation which describes the evolution of the interface. For more details about the formulation, our numerical contributions, and implementation in a GPU based code, see [13].

Validation of model

As a validation exercise for the model, let's explore the capillary force exerted on three solid gains at the coalescence of two initial menisci. This microscale force is representative of macroscopic strength of unsaturated media. The problem of coalescence of menisci was approached in the literature using an energy minimization technique [14] which will be herein compared with our LBM results.

The triplet configuration consists of two bottom particles separated by a distance of 8.3 mm with the upper particle at a distance of 8.7 mm from the centers of the bottom particles. All particles have the same radius of 4.4 mm. Two spherical water drops are initialized in the mid-segment one between the top and right particle, and the other between the top and right particle. If the seeded water volume is initially large, each capillary bridge will evolve on its own until at some point, coalescence of both bridges will occur to form one single merged capillary bridge at equilibrium when the imposed contact angle θ is satisfied.

Figure 1a shows the evolution of the two initial water menisci until equilibrium is reached, where a single merged liquid bridge is formed. A parametric study is performed by varying the initial water volume V from 1 to 33 μL, and contact angle θ for values of $20°, 40°, 50°$. The vertical capillary force F^{cap} exerted onto the upper particle is thus calculated to understand how capillary effects vary with water saturation.

Figure 1b shows a rather good agreement between LBM results and those based on energy minimization. However, what is most important here is the advantage of the LBM in computing forces such as those caused by adhesion, pressure and viscosity at every time step, while in the

energy minimization method, total forces are only calculated at equilibrium. Further what is most compelling is our capability of handling the dynamics of capillary bridges, which makes it extremely powerful for treating unsaturated granular assemblies, regardless of the capillary regime, whether with isolated or coalesced bridges.

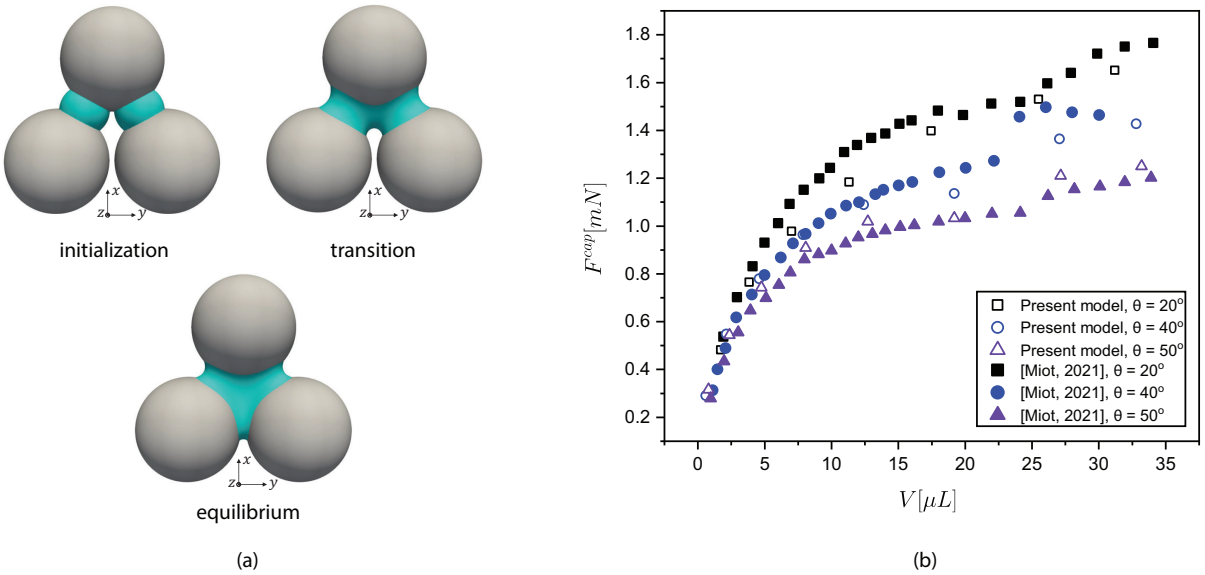

Figure 1: Liquid bridge dynamics in a triplet of particles: (a) merging of two initial menisci to form a large liquid bridge, (b) capillary force on upper particle as a function of the initial volume of the menisci and contact angle with comparisons with Surface Evolver used in [14]

Physics of Wetting and Drying

The physics of wetting and drying is next investigated in another case triplet of particles forming a equilateral triangle, but with the initial water menisci placed at all three contacts with a gap of 0.1 mm. To simulate evaporation and condensation during wetting and drying processes, the proposed algorithm is to perturb the phase field parameter ϕ at equilibrium by an infinitesimal amount so as to shift the position of the interface accordingly [15].

Figure 2a depicts the capillary forces evolution when the granular system is subjected to condensation followed by evaporation. As the volume of water increases, when the triple (three-phase contact) lines of the isolated capillary bridges touch each other, coalescence takes place, resulting into a transition from the pendular to the funicular regime. The merging occurs for a volume of $V \approx 10\mu L$ as seen Fig. 2a from state (a) to (b). It is important to note that at coalescence, a discontinuity in capillary forces is observed with a relatively sharp increase of 30% in capillary forces, which is completely in agreement with the theoretical value reported [16] for the same contact angle $\theta = 50°$.

To better understand the physics behind this sharp increase in capillary forces at coalescence, the evolution of the suction (difference between air and water pressures) force component and that due to surface tension are plotted in Fig. 2b. In the pendular regime and as the water

volume increases, it can be observed that suction force decreases continuously. By contrast, the surface tension force component increases because the wetting surface (solid-water interface) expands gradually around the particles. At coalescence, it is observed that the suction force suffers a significant jump (a→b) whereby it increases, whereas the surface tension force shows a slight decrease also through a jump (c→d).

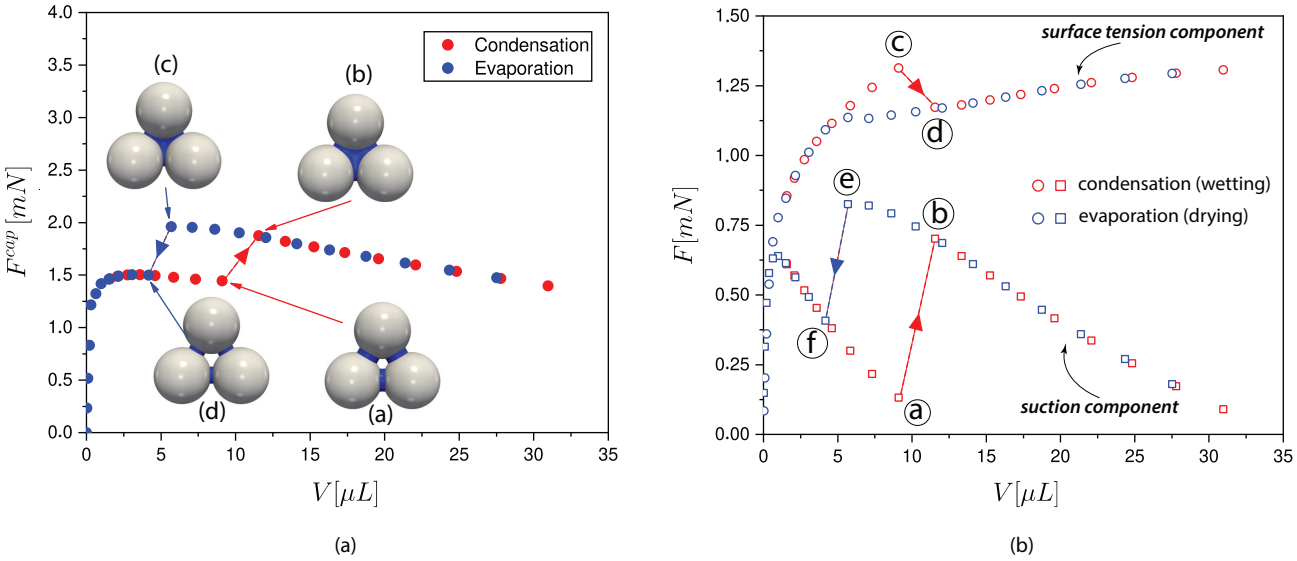

Figure 2: Force evolution as a function of water volume as the system is being wetted and dried using the condensation and evaporation algorithm: (a) total capillary force, and (b) surface tension and suction components

At the end of wetting when the water volume is $V = 30\mu L$, the evaporation process, i.e., drying, is thus initiated. The merged capillary bridge shrinks as evaporation proceeds until the water volume reaches $V = 6\mu L$ at step (c) in Fig. 2a. At this point, the capillary bridge spontaneously splits up into three smaller capillary bridges of equal size as seen in Fig. 2b at step (d). This rupture event causes a sharp decrease of 30.9% in the capillary force. Also, note that the volume at which bridges merge or split are different for the wetting and drying path, almost like representing a break in symmetry. Essentially, the jump in capillary force (sum of suction and surface tension components), seen in Fig. 2a for a wetting path, is purely of geometric origin. Hence, we may anticipate that the hysteresis of capillary forces during a wetting and drying cycle is strongly linked to pore scale mechanisms. These are in the form of a jump in force accompanying a sudden reconfiguration of the menisci during fluid filling or flushing of a pore throat, which will affect the strength of unsaturated soil during capillary transitions. One may surmise that these are instabilities germane to the well-known Haines jump observed in immiscible flow in porous media [17], but these need be further confirmed.

Coupled LB-DEM Simulations

To compute the formation of liquid bridges and their coalescence within a complex pore topology, the previously presented multi-component LBM equations in Eq. 4 are coupled with particle motions in DEM using the opensource code YADE [11]. As such, the fluid will evolve according to the discrete Boltzmann equations (Eq. 3) that will account for surface tension forces at fluid interfaces, the dynamics of which will be governed by the Allen-Cahn equation for an air/water composition based on density. From pendular to funicular and thereafter to full saturation, the evolution of distribution functions in LBM will translate into pressure, viscous and surface tension forces on the solid particles in a coupled manner [15]. In the end, stresses in an assembly of solid particles, water and air will be readily connected to deformations that ensue due to changes in capillary regimes during wetting, as will be illustrated next.

Sample setup

The granular assembly to be investigated consists of 3,750 spherical grains following a uniform grain size distribution such that $D_{max}/D_{min} = 1.35$ with $D_{max} = 108\mu m$ and $D_{min} = 80\mu m$. This ensures computational and capillary physics consistency, assuming a representative elementary volume in unsaturated media. As for the fluid phase, a total number of 10,877 spherical droplets are initialized between particles at a cutoff distance of $5\mu m$, which corresponds to approximately 10% of the maximum particle radius in the assembly. By growing or shrinking the size of the initialized spherical droplet radius, we thereby control the increase or decrease of the water saturation in the granular assembly as needed to explore the micro-physics of capillarity.

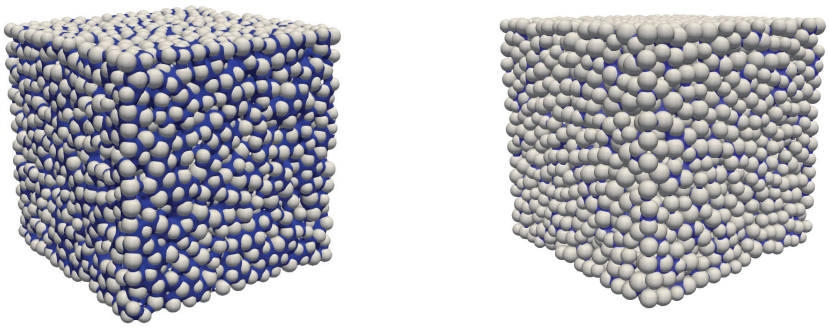

(a) (b)

Figure 3: (a) Initial configuration of a wet cubical sample confined within six walls. (b) Stable wet sample even after removing the lateral walls. The degree of saturation in this example is $S_r \approx 54\%$.

Figure 3a illustrates the initialization of a wet sample by sparsely spreading water droplets of a known total volume between the particles. After reaching both mechanical and thermodynamic equilibrium, the final distribution of liquid bridges is obtained. The liquid bridge topology corresponds to a specific homogenized suction field operating throughout the sample that allows it to stand freely, unconfined, as seen in Fig. 3b. Thus, the total stress on the

boundaries is zero with the granular (contact) stresses being in compression by virtue of the capillary stresses that have contributions from both suction and surface tension, see Figs. 1 and 2. Mathematically, the total stress $\boldsymbol{\sigma}$ can be decomposed into a contact stress $\boldsymbol{\sigma}^{cont}$ and a capillary stress $\boldsymbol{\sigma}^{cap}$ as: $\boldsymbol{\sigma} = \boldsymbol{\sigma}^{cont} + \boldsymbol{\sigma}^{cap}$.

The explicit form of the above stress equation has been worked out in [1, 6] in terms of microstructural information such as particle contact and liquid bridge topologies, contact forces, capillary forces, skin membrane surface tension, suction and interfaces. Stress contributions other than the contact stress are all lumped into the capillary stress. The contact stress which derives from particle contact forces and particle connectivity is calculated using the Love-Weber formula [18]. An important question that has been discussed in [8] is whether this stress is an effective stress in Terzaghi's sense for unsaturated soils which provides the basis of constitutive models.

Soil Water Characterisitic Curve—SWCC

A variety of interesting results concerning both retention and mechanical characteristics of unsaturated soils is herein explored to establish how matric suction and the capillary stress tensor evolve as a function of the degree of saturation.

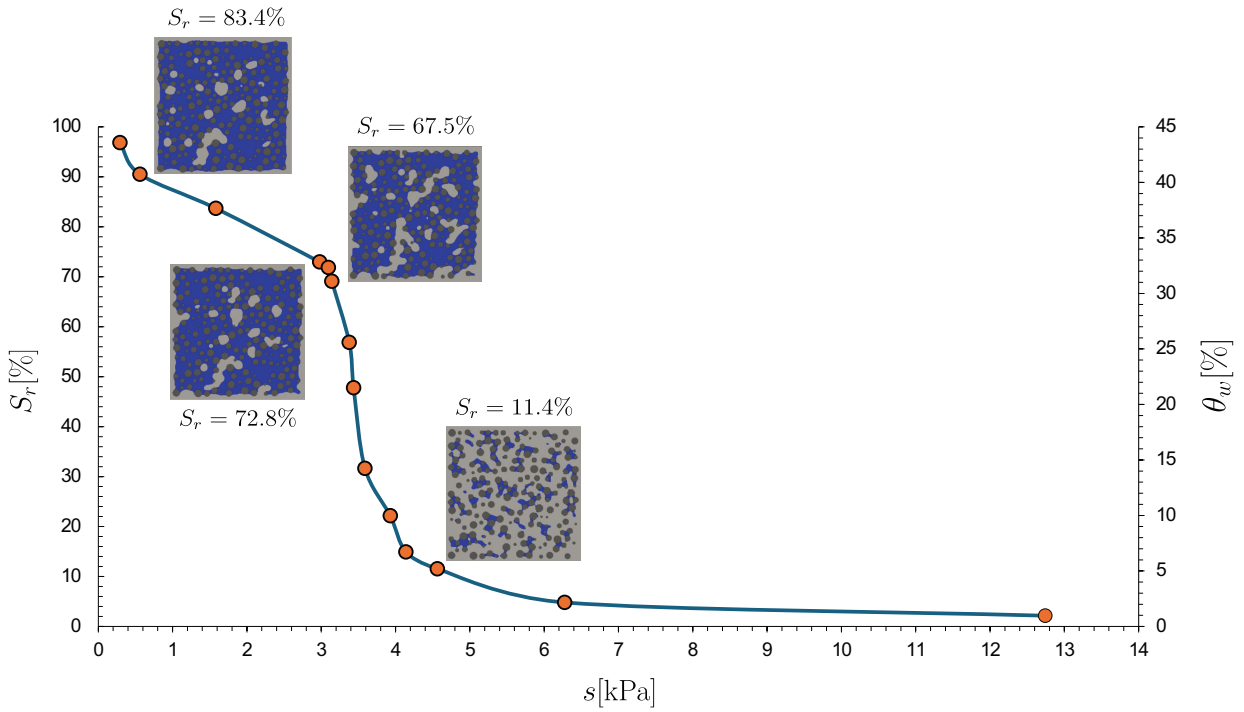

Figure 4: LBM-DEM computed SWCC showing snapshots of water and air distributions (2-D slices) at various transitions across the capillary regimes.

The computational procedure is as follows. Referring back to Fig. 3, the initial degree of saturation S_r as well as the volumetric water content θ_w can be computed knowing the porosity of the sample. In response to this water saturation, a matric suction s field develops from a

complex spatial distribution of clusters of menisci and air voids. These are homogenized into a single-valued s as the average of all local suctions s^i at capillary menici weighted by their respective volumes as in [19].

With a focus to microstructural details, Fig. 4 shows the computed SWCC with evolving air and water phases during a wetting process in the middle 2-D section of the cubical sample for clarity of illustration. At the beginning when $S_r = 11.4\%$, the wet granular assembly contains an extensive network of air clusters together with an invading large number of liquid bridges. As the degree of saturation increases to $S_r = 67.5\%$, isolated liquid bridges develop into one big cluster with a continuous air phase. This particular instance coincides approximately with the maximum curvature of the SWCC where suction starts to decreases appreciably. Upon further saturation, the originally continuous air phase dwindles to be reduced to ubiquitous trapped air bubbles as water will ultimately completely invades the pore space.

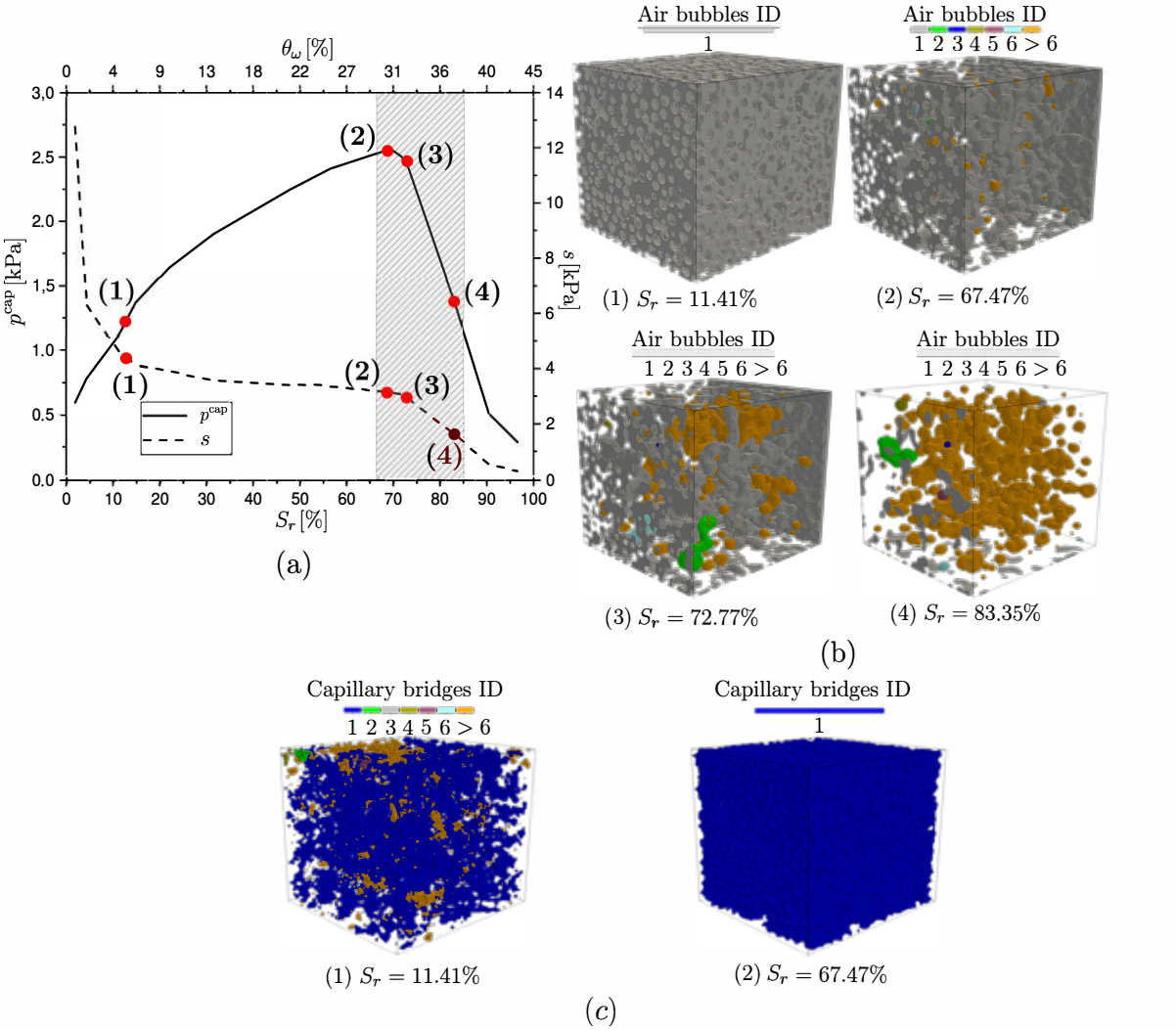

Figure 5: LBM-DEM computed SWCC showing snapshots of water and air distributions at various transitions across the capillary regimes.

We next explore the evolution of the mean capillary stress p^{cap} (one third of the first invariant of $\boldsymbol{\sigma}^{cap}$) superimposed onto that of suction s as a function of degree of saturation S_r and volumetric water content θ_w, see Fig. 5a. The air bubble and capillary bridge topologies are also plotted in Figs. 5b,c to help elucidate the evolution of p^{cap} and s, especially complement the previous 2-D interpretations in Fig. 4.

The post-processing of the numerical results involves using the flood-fill algorithm to detect capillary bridges and air bubbles, every one of which is labelled and given an ID. In Figs. 5b,c, since there is a myriad of entities to identify, only the first 6 ID's are shown so that anything above this cut-off value is represented by the same 'orange' colour. Against this backdrop, we find the general trend whereby the sample starts off with a low saturation of 11.4% at (1) with one predominately large cluster of air void living together with a large number of liquid bridges. With increasing saturation till (4), the air voids gradually decrease into smaller and smaller connected air during the ingress of water. The turning point is given by (2) where water begins to invade the pore space to expel the air as shown in Figs. 5b,c, focusing at point (2) with $S_r = 67.5\%$. It is interesting to note that this point coincides with the peak of the mean capillary stress and also the maximum curvature of the SWCC. In other words, the instant at which the capillary effects are the most intense is when water just enters the pore throats. Since we are concerned here with an unconfined sample, the contact stress tensor as a measure of effective stress is wholly compressive in opposition to the capillary stress tensor. Hence, the distinctive form of the p^{cap} vs. S_r curve shows the optimum saturation at which the soil is the strongest, which is familiar in the Proctor compaction test of soils.

Bishop's Equation

The description of stress conditions in unsaturated soil by Bishop's equation [20] has been a contentious issue connected to the existence of a Terzaghi-like effective stress that would control both the deformation and failure of unsaturated soils. There is a rich literature on this debate, starting with its origins in the 1960's [7] to more recent studies situated in micromechanical [1, 8] and thermodynamics frameworks to provide sufficiently general stress expressions, but yet no clearcut conclusions on the existence of an effective stress [21, 22]. Hence, in the light of our LBM-DEM simulations, it is tempting to examine the above-mentioned issues. To set the stage, we translate the familiar Bishop's effective stress equation, $\sigma - u_a = \sigma' - \chi s$, to identify the capillary stress in tensorial form as:

$$\boldsymbol{\sigma}^{cap} = \chi s\, \boldsymbol{I} = S_r s\, \boldsymbol{I}; \quad \boldsymbol{I} = \text{Identity tensor}$$

In the above, we note two simplifying assumptions made originally by Bishop, namely: (1) the isotropic (spherical) nature of the capillary stress, and (2) the assumption that the χ parameter is the degree of saturation S_r. In reality, the capillary stress tensor is bound to be non-spherical in nature, considering the anisotropy of contacts and liquid bridge distribution, which will be demonstrated next.

A comparision is proposed between p^{cap} as calculated from Bishop's equation and our LBM-DEM simulations where the capillary stress tensor can certainly be deduced by simple subtraction of the contact stress tensor from the total stress tensor. In line with the previous analysis,

mean capillary stress will increase until a certain optimum degree of saturation is reached beyond which the specimen starts to lose the effects of capillarity. In Fig. 6a, we can observe that p^{cap} based on Bishop's equation is always less than the LBM-DEM computed values. Despite the same tendency displayed in both curves, they do not match perfectly, especially before the optimum is reached. The reason for this lies in the assumption that $\chi = S_r$ noted earlier in Bishop's equation, which can be readily checked since the numerical simulations directly provide the actual value of the parameter χ [23], among others.

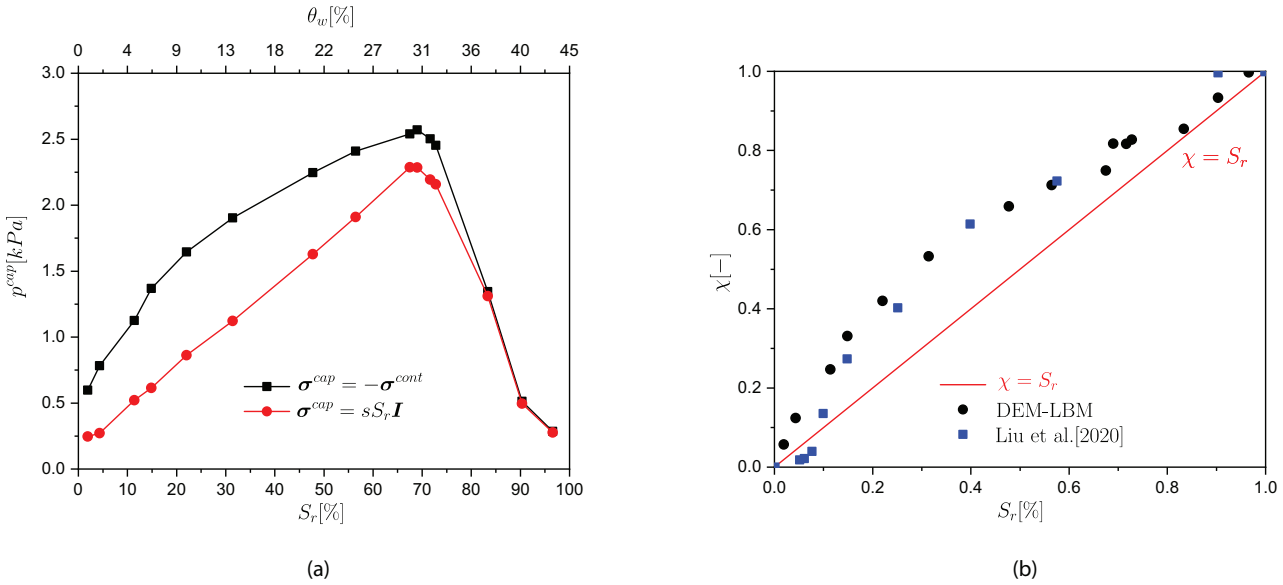

Figure 6: LBM-DEM computations versus Bishop's Equation: (a) mean capillary stress, (b) χ-parameter

Figure 6b shows the back-calculated χ plotted against S_r where χ and S_r almost never coincide. To confirm our findings, a numerical data set [24] has also been added. The two numerical results do not line up perfectly, especially for low levels of saturation less than 10% where $\chi < S_r$. This small discrepancy can be attributed to the difference between particle size distributions used in their work [24] and ours. Generally speaking, χ tends to remain greater than S_r as particle sizes increases, which makes our numerical results reasonable given the range of particle sizes we are using. Notwithstanding the above small discrepancies, the point is to demonstrate micromechanically that the χ-parameter cannot be confounded with the degree of saturation S_r, a fact that has been demonstrated experimentally on silt and clay, e.g. [23].

Conclusions

A synthesis has been presented of a numerical framework based on the coupling of particle-dynamics computer simulations for both solid grains and fluids (DEM and LBM) to decipher the underlying pore and grain scale physics of matric suction and surface tension during wetting and drying processes in unsaturated soils. To date, the description of the entire range of capillary regimes and transitions has mostly been phenomenological. In our work, reformulating

multiphase LBM to account for surface tension forces allows us to examine the dynamics of liquid bridges in complicated void space topology. As for describing wetting and drying processes, condensation and evaporation fluctuations are applied to the phase field that delineates the various phases.

The numerical simulations presented in the paper shed light on many longstanding issues related to capillarity effects as to their contributions to macroscopic strength and hysteretic behaviour during wetting and drying cycles. It is shown that there is a break in symmetry between wetting and drying cycles with the existence of jumps in the capillary forces during the reorganization of menisci, thus possibly representing local instability. Then, we can anticipate that transitions during the capillary regimes are dictated by small geometrical fluctuations that may grow depending on the pore topology which is in turn a function of mechanical stresses. These plausibly play a role in the strength of unsaturated soils under intermittent wetting and drying.

As for stress contributions in unsaturated soils, our numerical simulations confirm the limitations of Bishop's equation which is a widely accepted equation used in geotechnical engineering for unsaturated soils. Otherwise, stress partitioning in such multiphasic granular systems is tied to microstructure, suggesting that a more generalized tensorial stress expression [1] might be more appropriate as closely verified in [15].

To conclude, the success of the presented LBM-DEM model in capturing the complicated dynamics and hysteresis of liquid bridges over the entirety of saturation regimes makes it a plausible starting point for further development. In essence, the upscaling of the model via homogenization techniques will set forth rich continuum modelling of geostructures under fluctuating climatic loading dominated by wetting and drying cycles.

Acknowledgement

The first author is very grateful to all his co-authors who have contributed largely to this work within the IRN Geomech network. Gratitude is also due to the Natural Science Research Council of Canada (NSERC) for generous financial funding over the years.

References

[1] Jérôme Duriez, M Eghbalian, R Wan, and F Darve. The micromechanical nature of stresses in triphasic granular media with interfaces. *Journal of the Mechanics and Physics of Solids*, 99:495–511, 2017.

[2] R Wan, Jerome Duriez, and F Darve. A tensorial description of stresses in triphasic granular materials with interfaces. *Geomechanics for Energy and the Environment*, 4:73–87, 2015.

[3] D. G. Fredlund and H. Rahardjo. *Soil mechanics for unsaturated soils*. John Wiley & Sons, 1993.

[4] Delwyn G Fredlund. Unsaturated soil mechanics in engineering practice. *Journal of Geotechnical and Geoenvironmental Engineering*, 132(3):286–321, 2006.

[5] William J. Likos, Xiaoyu Song, Ming Xiao, Amy Cerato, and Ning Lu. *Fundamental Challenges in Unsaturated Soil Mechanics*, pages 209–236. Springer International Publishing, Cham, 2019.

[6] Mojtaba Farahnak, Richard Wan, Mehdi Pouragha, Mahdad Eghbalian, Francois Nicot, and Felix Darve. Micromechanical description of adsorptive-capillary stress in wet fine-grained media. *Computers and Geotechnics*, 137:104047, 2021.

[7] Alan W Bishop and GE Blight. Some aspects of effective stress in saturated and partly saturated soils. *Geotechnique*, 13(3):177–197, 1963.

[8] Jérôme Duriez, Richard Wan, Mehdi Pouragha, and Félix Darve. Revisiting the existence of an effective stress for wet granular soils with micromechanics. *International Journal for Numerical and Analytical Methods in Geomechanics*, 42(8):959–978, 2018.

[9] Mahdad Eghbalian, Mehdi Pouragha, and Richard Wan. Micromechanical formulation of first- and second-order works in unsaturated granular media. *International Journal for Numerical and Analytical Methods in Geomechanics*, 47(7):1152–1174, 2023.

[10] Timm Krüger, Halim Kusumaatmaja, Alexandr Kuzmin, Orest Shardt, Goncalo Silva, and Erlend Magnus Viggen. The lattice boltzmann method. *Springer International Publishing*, 10(978-3):4–15, 2017.

[11] Václav Šmilauer, Emanuele Catalano, Bruno Chareyre, Sergei Dorofeenko, Jerome Duriez, Anton Gladky, Janek Kozicki, Chiara Modenese, Luc Scholtès, Luc Sibille, et al. Yade reference documentation. *Yade Documentation 3rd ed.*, (1), 2021.

[12] Pao-Hsiung Chiu and Yan-Ting Lin. A conservative phase field method for solving incompressible two-phase flows. *Journal of Computational Physics*, 230(1):185–204, 2011.

[13] Nabil Younes, Z Benseghier, O Millet, A Wautier, F Nicot, and R Wan. Phase-field lattice boltzmann model for liquid bridges and coalescence in wet granular media. *Powder Technology*, page 117942, 2022.

[14] Marie Miot, Guillaume Veylon, Antoine Wautier, Pierre Philippe, François Nicot, and Frédéric Jamin. Numerical analysis of capillary bridges and coalescence in a triplet of spheres. *Granular Matter*, 23(3):1–18, 2021.

[15] N Younes, A Wautier, R Wan, O Millet, F Nicot, and R Bouchard. Dem-lbm coupling for partially saturated granular assemblies. *Computers and Geotechnics*, 162:105677, 2023.

[16] Gérard Gagneux and Olivier Millet. An analytical framework for evaluating the cohesion effects of coalescence between capillary bridges. *Granular matter*, 18(2):1–13, 2016.

[17] Zhonghao Sun and J. Carlos Santamarina. Haines jumps: Pore scale mechanisms. *Phys. Rev. E*, 100:023115, Aug 2019.

[18] Augustus Edward Hough Love. *A treatise on the mathematical theory of elasticity*. Cambridge university press, 2013.

[19] Jean-Yves Delenne, Vincent Richefeu, and Farhang Radjai. Liquid clustering and capillary pressure in granular media. *Journal of Fluid Mechanics*, 762, 2015.

[20] Alan W Bishop. The Principle of Effective Stress. *Teknisk ukeblad*, 39:859–863, 1959.

[21] N Khalili, F Geiser, and GE Blight. Effective stress in unsaturated soils: Review with new evidence. *International Journal of Geomechanics*, 4(2):115–126, 2004.

[22] Yimin Jiang, Itai Einav, and Mario Liu. A thermodynamic treatment of partially saturated soils revealing the structure of effective stress. *Journal of The Mechanics and Physics of Solids*, 100:131–146, 2017.

[23] J. E. B. Jennings and J. B. Burland. Limitations to the use of effective stresses in partly saturated soils. *Géotechnique*, 12(2):125–144, 1962.

[24] Xin Liu, Annan Zhou, Shui-long Shen, Jie Li, and Daichao Sheng. A micro-mechanical model for unsaturated soils based on DEM. *Computer Methods in Applied Mechanics and Engineering*, 368:113183, 2020.